Kiloamp High-Brightness Beams*

G. J. Caporaso
Lawrence Livermore National Laboratory, University of California
Livermore, CA 94550

Abstract

Brightness preservation of high-current relativistic electron beams under two different types of transport is discussed. Recent progress in improving the brightness of laser-guided beams in the Advanced Test Accelerator is reviewed. A strategy for the preservation of the brightness of space-charge-dominated beams in a solenoidal transport system is presented.

Introduction

High-brightness, or low-emittance, high-current relativistic electron beams are of interest for a variety of applications. We discuss emittance growth of such beams under two very different transport schemes.

In the case of laser-ion guiding, the space-charge field of the beam is dominated by the electrostatic field of the ion channel that governs any emittance growth in this transport mode.

Many researchers have seen emittance growth of intense ion beams in conventional magnetic focusing systems caused by nonlinear space-charge forces in the results of particle code calculations. Whenever the dimensionless beam intensity given by $I/((\gamma\beta)^3 I_0 K_c E)$ is of order 1, nonlinear space-charge forces may give rise to emittance growth. Here I and I_0 are the beam current and 17 kA, respectively, and K_c and E are the cyclotron wavenumber and unnormalized emittance, respectively. This regime is entered when conventional solenoidal transport is used to guide low-emittance, high-current relativistic electron beams at energies of several MeV. We will present strategies for each type of transport system that minimize emittance growth in linear accelerators.

Laser Ion Guiding

Laser-ion guiding has proven to be highly effective at suppressing transverse beam motion arising from instabilities in ATA at beam currents up to 10 kA.[1] These beneficial effects arise primarily from the nonlinear nature of the guiding force provided by the channel that leads to phase-mix damping of any coherent beam motion. This same property of the channel can also lead to severe emittance growth. Initial observations suggested that the beam emittance at the downstream end of the accelerator was larger than expected on the basis of measurements of beam emittance at the injector.[2]

We will address problems of matching the beam from a magnetic channel onto the ion channel, then focus on the ion-hose instability in the context of possibly explaining the observed apparent increase in emittance of the beam as a function of time through the pulse.

In ATA, the beam is magnetically guided from the injector up to the matching region where the transition to ion-channel guiding occurs. The matching region in ATA typically extends over one or two cell blocks (approximately 3.5 to 7 m). The benzene pressure is tapered over this region from less than $\approx 0.005\ \mu$ at the upstream end to $\approx 0.07\ \mu$ at the downstream end. The downstream end is defined to be that location where the axial magnetic field that is tapered from a relatively high value upstream (≈ 1 kG) is reduced to zero. Figure 1 depicts this region.

A feature observed on nearly all shots using laser guiding is a loss of current on the downstream conductance limiter. This limiter was a 2-in.-diam, approximately 50-cm-long pipe over which it had been planned to reduce the benzene pressure to enable the beam to propagate in a quadrupole lattice up to various experiments. However, even with full benzene pressure ($\approx 0.1\ \mu$) in the limiter, some current was lost. The loss of current was most severe at the tail of the pulse. This observation is in accord with the results of gated TV pictures of the light from foils placed in the downstream beamline, which show an apparent growth of beam size through the pulse. Figure 2 shows the inferred beam radius at the downstream end of ATA as a function of time through the pulse.

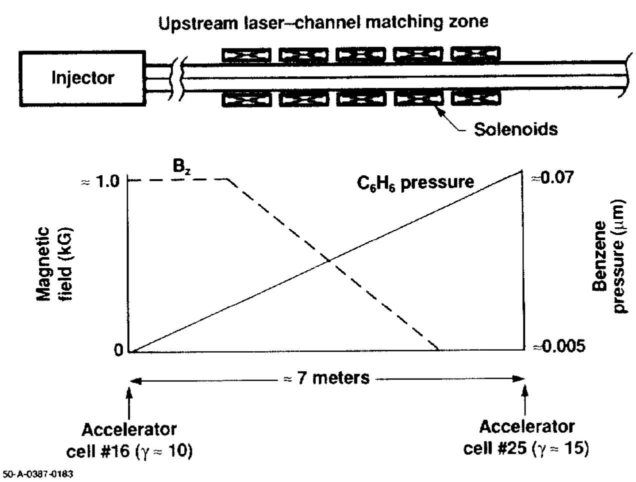

Fig. 1. Schematic of the upstream matching region showing approximate location and axial field and benzene pressure profiles. There are no solenoidal fields downstream of this region.

In trying to match the beam from magnetic focusing onto the channel, the axial magnetic profile is adjusted so that the combined focusing strength of solenoids and channel in the matching region is approximately constant and equal to the upstream value of the solenoids alone. This value is also equal in strength to that of the channel at the downstream end of the matching zone. This channel strength is usually sufficient to result in an equilibrium RMS radius that is less than the channel radius.

One may define an effective potential of the solenoidal channel as $k_c^2 r^2/8$, where k_c is the cyclotron wavenumber. For a uniform channel of radius a, the effective potential is $k_\beta^2 r^2/2$ for $r < a$ and $k_\beta^2 a^2\ [1 + 2\ln(r/a)]/2$ for $r > a$ where k_β^2, the square of the betatron wavenumber, $\approx 2e\lambda/(\gamma\beta^2 mc^2 a^2)$. Here λ is the linear charge density of the channel. To obtain a good match, the channel strength is adjusted so that k_β at the downstream end of the

*Work performed jointly under the auspices of the U.S. Department of Energy by Lawrence Livermore National Laboratory under contract W-7405-ENG-48, for the Strategic Defense Initiative Organization and the U.S. Army Strategic Defense Command in support of SDIO/SDC-ATC MIPR No. W31RPD-7-D4041.

CH2387-9/87/0000-1001 $1.00 © IEEE
PAC 1987

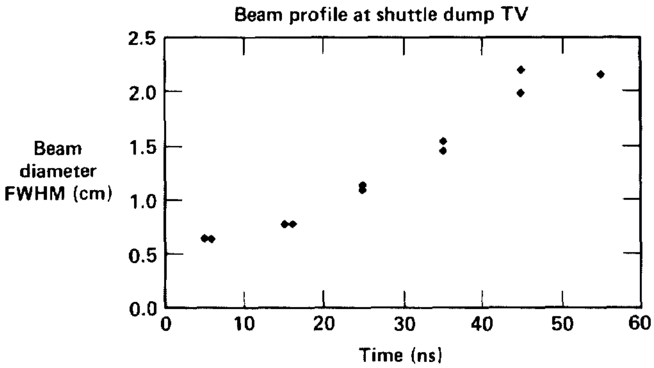

Fig. 2. Beam radius as a function of time through the pulse. The radius is the full width at half-maximum of the light observed when the beam impinges on a graphite foil at the downstream end of the accelerator. The light from the foil is observed on a TV camera with a 10-ns gate.

matching zone $\approx k_c/2$ at the upstream end of the matching zone.

We note that since the potential outside the channel has a logarithmic dependence on radius while the magnetic potential is quadratic for all radii, the potential is extremely soft outside the channel as compared to the potential of a solenoid with $k_c/2 = k_\beta$. The transition from magnetic focusing to ion focusing must be made with care. Any injection mismatch errors or transverse kicks to the beam sufficient to drive electrons out of the channel can result in very large electron orbit excursions from the axis because of the soft potential. The maximum electron orbit radius is exponentially sensitive to the size of the kick. These large orbit excursions can lead to current loss on the wall and emittance growth because the resulting large beam radial or transverse displacements will phase mix damp.

Ion-Hose and the Growth of Emittance with Time

The ion-hose instability has been studied by a variety of analytical and numerical approaches.[3,4] It is a transverse instability that arises from the electrostatic coupling of the beam-channel system and the fact that on the time scale of the beam pulse the ions are mobile. Most of the theoretical approaches to this instability have predicted that the ion-hose would grow (until saturation) with axial distance from the initiation of a disturbance. When this instability was not observed either in ATA or in the downstream transport region even when the beam was deliberately deflected, we began to search for stabilizing mechanisms. We found one such mechanism. The channel created by the beam-induced ionization of the benzene was found to stabilize the ion-hose in the sense that for a beam injected onto a channel with a transverse angle the beam displacement would grow for several betatron wavelengths and then damp.[4] Slices of the beam progressively further back from the head would undergo the same growth pattern with larger amplitudes; but in all cases the disturbance would not propagate axially. The disturbance is confined to a region a few betatron wavelengths long, and the peak amplitude of the disturbance is a monotonically increasing function of the distance back from the head of the beam.

We performed a non-self-consistent calculation to test the idea that the stabilized ion-hose occurring in the upstream matching region was the cause of the observed increase of beam size as a function of time through the pulse. We ran an ion-hose code with a mobile beam-induced channel[4] using values for channel charge and size appropriate for the ATA matching region. We assumed that the beam was injected onto the channel with a transverse angle of 0.001 radians, which corresponds to the measured angle of the applied magnetic field with respect to the axis of the accelerator. This angle is caused by transverse error fields in the solenoids.

The ion-hose code outputs the transverse channel position as a function of axial distance for different slices of the beam. For each slice, we placed the transversely displaced channel into the single-disk particle code called WIRE.[5] We then ran the disk of electrons through the rippled ion channel to compute emittance growth and radius increase for that slice. An output sample is shown in Fig. 3. The results are in reasonable quantitative agreement with the observations on ATA and are displayed in Fig. 4.

Recently, a new matching technique has been employed on ATA for low-current (several-kA), low-emittance transport. The matching apparatus is shown in Fig. 5. The essence of the technique is to match onto the channel inside of a magnetic emittance selector that is located at the output of the injector. The emittance selector is a 1.06-m-long, 1-cm-radius pipe with solenoids over it. Benzene is fed into the system at the downstream end while a large-capacity vacuum pump is attached to the upstream end. This arrangement results in a linear pressure drop across the selector on the order of a factor of 25. In operation, the solenoid strengths over the selector are tapered in the opposite sense to the pressure so as to approximate a constant-strength channel over the entire length of the selector. All solenoids downstream of the selector are turned off. The upstream channel size at the location of the selector is 12 x 20 mm, so that the channel is nominally the same size as the pipe.

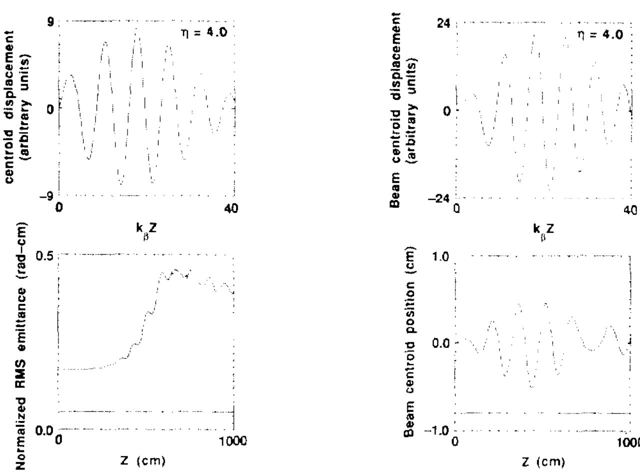

Fig. 3. Results of the ion-hose emittance growth calculations. The (a) and (b) plots from the ion-hose code show the channel and beam centroid positions, respectively. These results must be multiplied by $0.001/k_\beta$ to yield displacements in cm. The horizontal axis is the dimensionless distance $k_\beta z$. The (c) and (d) plots show the results from the WIRE transport (particle) code for RMS emittance and beam centroid position in radian-cm and cm, respectively, for propagation of a disk through the rippled channel provided by the ion-hose code output. The horizontal axes are axial distances in cm. In plots (c) and (d), 857 cm corresponds to $k_\beta z = 40$ in plots (a) and (b). Agreement is excellent between the beam centroid positions found from the two codes. These calculations were run for the slice $\eta = \omega_0 \tau = 4$ (ω_0 is the ion-sloshing frequency in the electrostatic field of the beam).

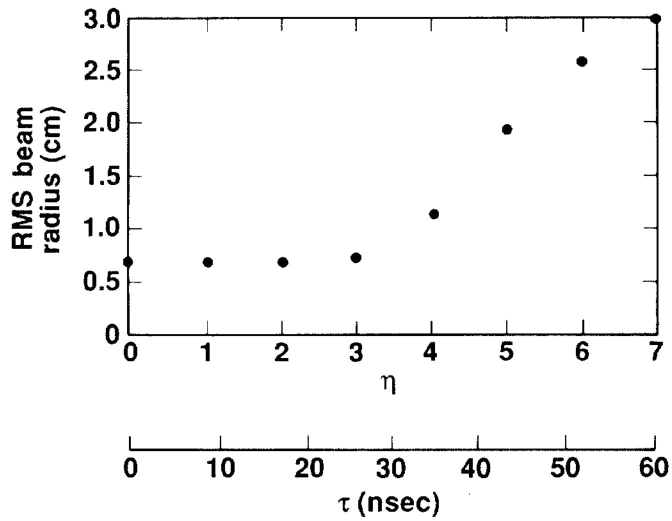

Fig. 4. Plot of the final RMS beam radius for different slices as found from the WIRE transport code using the channel positions computed in the ion-hose code. The results are in good agreement with observations. An interesting feature of the calculation is that it correctly predicts the time required for significant growth of the beam radius.

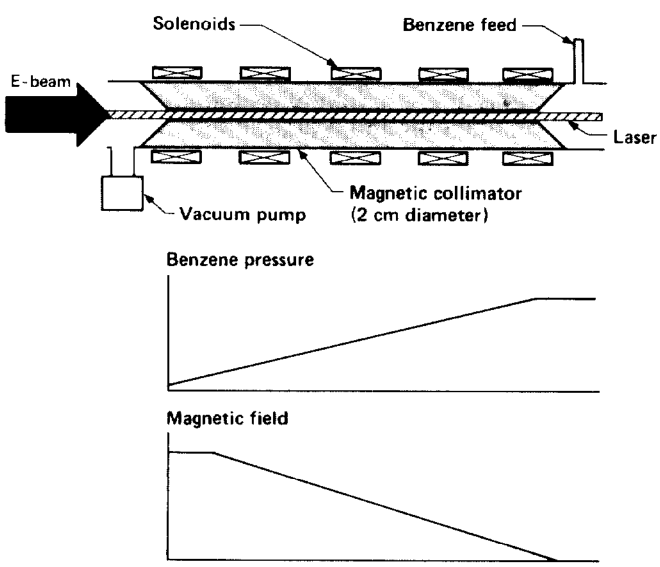

Fig. 5. Schematic of the new matching zone recently installed and tested on ATA showing the pressure and approximate magnetic field profiles used in the device. The inner pipe of the zone is 1 cm in radius and 106 cm long. The pipe is almost the same size as the laser "footprint" so that the beam emerging from the zone is totally within the channel. The collimation provided by the zone ensures that there is no transverse centroid displacement of the transmitted beam. Typically 9 kA is incident on the pipe and 2 kA passes through. The measured brightness of the beam at the downstream end of ATA has been improved by a factor of 5-10 using this technique up to a value of at least 1.3 x 10^5 for 2000 A.

Usually ≈ 9 kA addresses the selector and ≈ 2 kA passes through. The current that does pass through is forced to be inside the channel. Likewise, there is no transverse displacement of the beam because this is also prevented by the collimation of the selector. Radial mismatch of the beam is also minimized: when the output current of the collimator is maximized, the match of the beam to the channel is optimum.

Use of this technique has resulted in an improvement in the measured brightness of the beam at the end of ATA by a factor of 5-10. In addition, current loss is now not observed on the downstream conductance limiter. Measurements performed downstream of ATA show that approximately 2 kA can be obtained at a brightness of at least 1.3 x 10^5 A/cm^2-steradian and is close to the value of brightness measured at the output of the injector.[6]

Solenoidal Guiding

Many papers beginning with the pioneering work of Lapostolle[7] have shown that the brightness of space-charge-dominated beams decreases during transport because of the effects of nonlinear space-charge forces.[8,9]

Recently it has been shown that part of this brightness decrease results from the conversion of excess space-charge potential energy into effective thermal transverse kinetic energy.[9]

The magnitude of the potential energy is a function of the beam radial profile and will be shown to be independent of the beam size. In any transport process occurring at constant RMS radius, the difference between the space-charge potential energy of the beam in the initial and final configurations is transferred into effective thermal transverse kinetic energy. The emittance growth during this process is related to the product of the increased effective thermal transverse RMS velocity and the RMS beam radius. If the radius is held to a small value during the process, then the emittance growth is minimized. In this sense, the increase in emittance caused by space-charge forces is analogous to the increase of emittance caused by passage of a beam through a thin scattering foil. The foil provides an increase in the transverse velocity of the beam particles that is independent of the beam size. The emittance change, however, depends on the beam size.

We may derive an equation for the change of RMS emittance by following the methods of Refs. 8 and 10. We start with the envelope equation for the RMS radius of a cylindrically symmetric beam in a solenoidal field:[10]

$$R'' = -\frac{\gamma' R'}{\gamma\beta^2} + \frac{E^2}{R^3} + \frac{I}{(\gamma\beta)^3 I_0 R} - \frac{1}{4} k_c^2 R \quad , \qquad (1)$$

where we have taken the beam to have zero canonical angular momentum P_θ, and where E is the RMS emittance. Here I is the beam current, $I_0 = mc^3/e \approx 17$ kA, and k_c is the cyclotron wavenumber $eB/(\gamma\beta mc^2)$. We use the definition of emittance,

$$E^2 = R^2[V^2 - R'^2 - L^2/R^2] \quad , \qquad (2)$$

where L, the mechanical angular momentum, is equal to $k_c R^2/2$ for a beam with $P_\theta = 0$, and where V is the RMS transverse velocity normalized to c, the speed of light. A prime denotes differentiation with respect to z, the axial distance. Differentiation of Eq. (2) leads to

$$\frac{\partial E^2}{\partial z} = R^2 \frac{\partial V^2}{\partial z} + \frac{2\gamma' R^2 R'^2}{\gamma\beta^2} - \frac{1}{2} R^4 k_c k_c' - \frac{2IRR'}{(\gamma\beta)^3 I_0} \quad . \qquad (3)$$

Now consider the single particle force equation

$$\beta mc^2 \frac{\partial}{\partial z}\left(\gamma\beta \frac{\partial\vec{r}}{\partial z}\right) = \frac{2eI_r}{\gamma^2\beta cr}\hat{e}_r - e\beta B \frac{\partial\hat{r}}{\partial z} \times \hat{e}_z - e\beta\hat{e}_z \times B_r\hat{e}_r$$

where

$$I_r \equiv \int_0^r 2\pi r J_z \, dr$$

is the current enclosed at radius r and appears in the term representing the space-charge force. $B = B_{zs}$ and $\vec{\nabla} \cdot \vec{B} = 0$ imply that $B_r \approx -r/2(\partial B/\partial z)$. If we dot $\partial r/\partial z$ into the single-particle force equation, we obtain

$$\frac{1}{2}\frac{\partial}{\partial z}\left(\frac{\partial\vec{r}}{\partial z}\right)^2 + \frac{\gamma'}{\gamma\beta^2}\left(\frac{\partial\vec{r}}{\partial z}\right)^2 = \frac{2I_r V_r}{(\gamma\beta)^3 I_0 r} + \frac{1}{2}k_c\frac{B'}{B} rV_r \quad , \tag{4}$$

where $v_r = \hat{e}_r \cdot \overrightarrow{\partial r}/\partial z$ and $v_\theta = \hat{e}_\theta \cdot \overrightarrow{\partial r}/\partial z$. We now average this equation over the beam profile using the prescription

$$\langle A\rangle = I_1 \int_0^{a_b} 2\pi r J_z A \, dr \quad ,$$

where a_b is the beam edge radius.

We assume $\gamma\beta$ to be constant across the beam radius and we employ the local averaging procedure of Ref. 6 to obtain the beam-averaged quantities $\langle I_r v_r/r\rangle$ and $\langle rv_\theta\rangle$ as $\langle I_r u_r/r\rangle$ and $\langle ru_\theta\rangle$, respectively. Here u_r (u_θ) is the local mean radial (azimuthal) velocity. Now, using these results, Eqs. (1) and (2), and noting that $\langle ru_\theta\rangle = L = k_c R^2/2$, Eq. (4) becomes

$$\frac{\partial E^2}{\partial z} + \frac{2\gamma' E^2}{\gamma\beta^2} = \frac{2R^2}{(\gamma\beta)^3 I_0}\left[2\left\langle\frac{I_r u_r}{r}\right\rangle - \frac{IR'}{R}\right] \quad . \tag{5}$$

The quantity $\langle I_r u_r/r\rangle$ may be rewritten by using the continuity equation cast in the form[6] $\partial J_z/\partial z + 1/r^2/\partial r(rJ_z u_r) = 0$, which may be integrated to give

$$\partial I_r/\partial z + 2\pi r J_z u_r = 0 \quad . \tag{6}$$

Using Eq. (6), we find that

$$\langle I_r u_r/r\rangle = -1/2 \int_0^{a_b} \partial/\partial z(I_r/I)^2 \, dr/r \quad .$$

Noting that the normalized RMS emittance $E_n = \gamma\beta E$ and defining $\xi \equiv r/R$, $g(z,\xi) \equiv I_r(z,\xi)/I$, $\xi_b(z) = a_b(z)/R(z)$, we can rewrite Eq. (5) as

$$\frac{\partial E_n^2}{\partial z} = -\frac{2IR^2}{\gamma\beta I_0}\left[\frac{\partial}{\partial z}\int_0^{\xi_b(z)} \frac{d\xi}{\xi} g^2(\xi) - \frac{\xi_b'}{\xi_b} + \frac{R'}{R}\right] \quad , \tag{7}$$

where we have extracted the operator $\partial/\partial z$ from inside the integral.

We now consider the transport of a coasting beam (i.e., one which is not undergoing acceleration) in which $R' = 0$ but which involves a change in radial profile from one form at $z = 0$ to a different asymptotic form as $Z \to \infty$. Under these conditions, Eq. (7) may be integrated to yield

$$E_n^2(\infty) = E_n^2(0) + \frac{2IR^2}{\gamma\beta I_0}\left[\int_0^{\xi_b(0)} \frac{d\xi}{\xi} g^2(0,\xi) - \int_0^{\xi_b(\infty)} \frac{d\xi}{\xi} g^2(\infty,\xi) - \ln\left\{\frac{\xi_b(0)}{\xi_b(\infty)}\right\}\right] \quad . \tag{8}$$

This result is similar to that found heuristically in Ref. 5. Equation (8) explicitly displays the dependence of the emittance growth on the beam radius. The dimensionless quantity in brackets depends only on the initial and final beam shape.

We may write Eq. (9) as $E_n^2(\infty) = E_n^2(0) + R^2\theta_{S\perp}^2$, where

$$\theta_{S\perp}^2 = \frac{2I}{\gamma\beta I_0}\left[\int_0^{\xi_b(0)} \frac{d\xi}{\xi} g^2(0,\xi) - \int_0^{\xi_b(\infty)} \frac{d\xi}{\xi} g^2(\infty,\xi) - \ln\left(\frac{\xi_b(0)}{\xi_b(\infty)}\right)\right] \quad ,$$

and is equal to twice the change in the space-charge potential energy. We can compare this to the emittance change of a beam passing through a scattering foil given by $E^2(z_2) = E^2(z_1) + R^2\theta_s^2$ where θ_s^2 is the mean squared scattering angle imparted to the beam electrons and z_2 and z_1 are positions downstream and upstream of the foil, respectively.

We note that $\theta_{S\perp}^2$ is dependent only upon the initial and final profile shapes and not upon the beam radius. This result suggests that $E_n^2(\infty)$ can be minimized by letting the transport occur at the smallest radius possible.

This concept was tested in a particle simulation of the transport of an intense relativistic electron beam through tens of meters of solenoidal transport. The calculation begins at the cathode of an injector using the particle code DPC.[11] A single axial slice of the beam is then passed to the WIRE transport code 32 cm downstream of the cathode. The 3-kA beam emerges from the 3-MeV injector and is transported at two different radii. In the first case, the solenoids are adjusted to maintain a constant RMS beam radius, while in the second case the beam is matched into a 3-kG solenoidal channel at a substantially reduced radius.

Figure 6a is a plot of the RMS radius vs axial distance for 30 m of propagation for the first case. The corresponding normalized RMS emittance vs axial distance is shown in Fig. 6b. Figure 7a shows the RMS radius vs axial distance for the second case, which involves a match into a 3-kG field. The corresponding emittance plot is given in Fig. 7b. In both cases the beam propagates a significant distance at relatively constant RMS radius. Emittance growth is observed to occur in both cases and saturates because the beam achieves an asymptotic radial profile. The growth of emittance for the case of small-beam radius is substantially less than in the large-radius case.

The pinch-down occurs in a distance that is short compared to an upstream betatron wavelength, and the calculation shows that the emittance is preserved in that transition, although the general conditions under

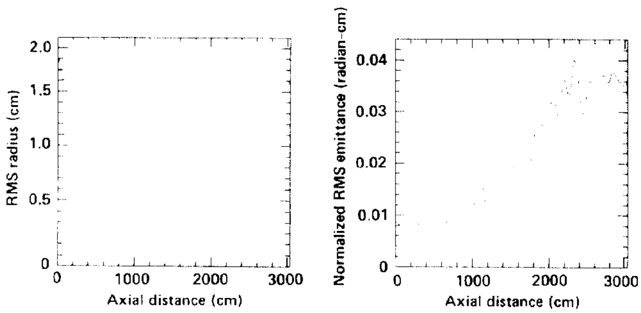

Fig. 6. (a) RMS beam radius vs axial distance for the first transport case corresponding to the larger beam radius. (b) Normalized emittance vs axial distance showing large emittance growth and saturation. The emittance growth stops when the beam achieves an asymptotic radial profile.

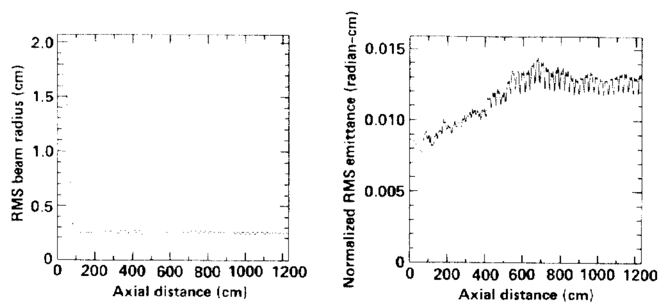

Fig. 7. (a) RMS radius vs axial distance for the case of a match into a high-strength solenoidal field. (b) RMS normalized emittance vs axial distance showing emittance growth and saturation. The growth in emittance for this case is significantly smaller than for the large-radius case shown in Fig. 6.

which this is possible remain an open question. Beyond the pinch-down region, Eq. (8) is applicable.

Conclusions

We have developed a technique that allows transport of several kiloamperes through an induction linac using laser guiding with almost no emittance growth. In addition, we present a theoretical technique for minimizing the emittance growth of space-charge-dominated beams under solenoidal guiding. The technique differs from conventional adiabatic change in beam size and axial magnetic field by prescribing a rapid decrease of beam radius. Quickly attaining small-beam radius ensures that the emittance growth caused by the conversion of space-charge potential energy into effective thermal transverse kinetic energy will be minimal.

References

1. G. J. Caporaso, F. Rainer, W. E. Martin, D. S. Prono, and A. G. Cole, Phys. Rev. Lett. 57, 1591 (1986).
2. Y. P. Chong et al., Beam Profile of the Advanced Test Accelerator Under Laser-Ion Guiding, LLNL Report UCRL-93751 to be published in the Proceedings of BEAMS '86, the 6th International Conference on High-Power Particle Beams, June 9-12, 1986, Kobe, Japan.
3. H. L. Buchanan, Linear and Non-Linear Calculations of the Hose Instability in the Ion Focused Regime, LLNL Report UCID-19495, 1982.
4. G. J. Caporaso, A. G. Cole, and E. J. Lauer, IFR Hose Theory, LLNL Report UCRL-92874 (1985).
5. G. J. Caporaso and A. G. Cole, IEEE Trans. Nucl. Sci., NS-30 (4), 2610 (1983).
6. J. T. Weir, J. K. Boyd, G. J. Caporaso, and T. Orzechowski, "Experimental Results of Beam Brightness Improvements at ATA" to be published as paper H11 for this conference.
7. P. M. Lapostolle, IEEE Trans. Nucl. Sci., 18, 1101 (1971).
8. E. P. Lee, S. S. Yu, and W. A. Barletta, Nucl. Fusion 21, 961 (181).
9. J. Struckmeier, J. Klabunde, and J. Reiser, Part. Accel. 15, 47 (1984).
10. E. P. Lee and R. K. Cooper, Part. Accel. 7, 83 (1976).
11. J. K. Boyd, G. J. Caporaso, and A. G. Cole, IEEE Trans. Nucl. Sci., NS-32 (5), 2602 (1985). J. K. Boyd, Proc. of the 7th Int. Free Electron Laser Conf., Nucl. Instr. and Methods A249 (1986), in press.